Voltammetric Monitoring of Gold Nanoparticle Formation Facilitated by Glycyl-L-Tyrosine: Relation to Electronic Spectra and Transmission Electron Microscopy Images

J. M. Booth,[†] S. K. Bhargava,*[,‡] A. M. Bond,[§] and A. P. O'Mullane[§]

Commonwealth Scientific and Industrial Research Organization, Manufacturing and Infrastructure Technology, Locked Bag 33, Clayton South, Victoria 3169, Australia, Advanced Materials and Catalysis Group, School of Applied Sciences (Applied Chemistry), Science, Engineering and Technology Portfolio, RMIT University, Melbourne, Australia, and Electrochemistry Group, School of Chemistry, Monash University, Melbourne, Australia

Received: March 27, 2006; In Final Form: May 9, 2006

Voltammetric techniques have been introduced to monitor the formation of gold nanoparticles produced via the reaction of the amino acid glycyl-L-tyrosine with Au(III) (bromoaurate) in 0.05 M KOH conditions. The alkaline conditions facilitate amino acid binding to Au(III), inhibit the rate of reduction to Au(0), and provide an excellent supporting electrolyte for voltammetric studies. Data obtained revealed that a range of time-dependent gold solution species are involved in gold nanoparticle formation and that the order in which reagents are mixed is critical to the outcome. Concomitantly with voltammetric measurements, the properties of gold nanoparticles formed are probed by examination of electronic spectra in order to understand how the solution environment present during nanoparticle growth affects the final distribution of the nanoparticles. Images obtained by the ex situ transmission electron microscopy (TEM) technique enable the physical properties of the nanoparticles isolated in the solid state to be assessed. Use of this combination of in situ and ex situ techniques provides a versatile framework for elucidating the details of nanoparticle formation.

1. Introduction

In line with the intense focus of research activities on nanotechnology apparent over the past decade or so, nanoparticles of gold have been viewed as having significant potential for remarkably varied applications. For a summary of this potential with respect to applications such as sensing technology, catalysis, and nonlinear optics and a comprehensive introduction to gold nanoparticle synthesis, the reader is directed to the review of Daniel and Astruc.[1] Given the attention received, it is not surprising that there has been a proliferation of synthetic methods reported in recent years. Of particular interest for biotechnological applications are syntheses involving biogenic agents such as lemongrass,[2] aloe vera,[3] actinomycetes,[4] proteins,[5] and amino acids.[6−8] Such agents provide possibilities for inexpensive production of biofunctionalized gold nanoparticles on large scales which have tailored morphologies and, therefore, properties.[9]

Turkevich et al.[10] reported that the production of gold nanoparticles by the citrate method proceeds by initial formation of clusters of citrate cross-linked with Au(III), followed by a temperature-dependent induction time corresponding to the conversion of the citrate molecules into acetone dicarboxylate. Chow and Zukoski[11] also explored the formation of gold nanoparticles via the citrate method and found that the large gold clusters formed at early reaction time subsequently decomposed into dispersions of smaller particles.

In view of the similar number of electron-donating groups, a mechanism related to that postulated by Turkevich et al.[10] for the citrate process might be expected to occur when nanoparticles are formed by the reaction of gold with simple amino acids. The citrate studies have focused on aspects of the early stages of nanoparticle formation. In contrast, studies in the peptide area have probed the final stages so that mechanistic details of the significant earlier stages in the reduction process remain unexplained. In the present study, electrochemical methods are introduced into mechanistic studies, to be able to monitor all stages of the formation of gold nanoparticles generated by the reduction of bromoaurate ($AuBr_4^-$) in the presence of glycyl-L-tyrosine (Structure 1) under alkaline (0.05 M KOH) conditions.

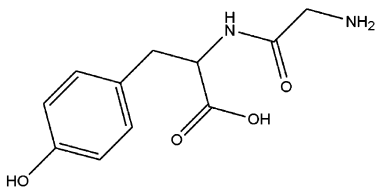

Structure 1: Glycyl-L-tyrosine

The necessity of having 0.05 M KOH present is fortunate, as this provides an excellent supporting electrolyte for voltammetric studies. This technique allows the possibility of electrochemically monitoring the consumption of reactants and the formation of products as a function of time. Voltammetric measurements also are sensitive to the chemical environment of solution-soluble species so that changes in composition of intermediates also can be monitored.

* To whom correspondence should be addressed. E-mail: suresh.bhargava@rmit.edu.au. Phone: +61 3 99253365.
[†] Commonwealth Scientific and Industrial Research Organizatio.
[‡] RMIT University.
[§] Monash University.

10.1021/jp061896i CCC: $33.50
Published on Web 06/08/2006

Previously, studies in the nanoparticle field have described the direct electrochemical syntheses of gold nanoparticles in the presence of a capping agent[12,13] and the quantized double layer charging phenomenon associated with alkanethiol capped gold nanoparticles.[14−18] However, the present study appears to be the first time electrochemical methods have been employed to monitor the course of reactions that occur prior to gold nanoparticle formation, when gold(III) solutions are reduced by a dual chemical reductant/capping agent.

UV−visible spectroscopy is a well established in situ technique for probing the properties of gold nanoparticles produced in a dynamic solution environment. These data generate complimentary information to that provided by voltammetric techniques, which elucidate details of the nature of the solution environment. Transmission electron microscopy (TEM) is another extensively used technique in the area of nanoparticle characterization. This ex situ technique probes the properties of nanoparticles in the absence of a surrounding solution and provides a snapshot of the solid formation at a particular time. Access to results from these three techniques enable the course of nanoparticle formation to be monitored from the time when the initial precursor solutions are mixed together, through intermediate stages of reaction, right through to the final isolated solid nanoparticle material.

2. Materials and Method

2.1. Chemicals. Potassium tetrabromoaurate was prepared by the direct bromination of gold powder in the presence of potassium bromide. Potassium hydroxide (laboratory-reagent grade) was obtained from Merck. All amino acids used were of laboratory-reagent grade or better and of the L-stereochemical configuration. Distilled water used in the preparation of the nanoparticle dispersions was purified with a Millipore filter (resistivity 18.2 MΩ cm).

2.2. Synthesis of Gold Nanoparticles. Two methods were employed for the synthesis of gold nanoparticles:

2.2.1. Method A. The required mass of amino acid was added to 10 mL of aqueous 0.1 M KOH to give a 1 mM solution. 0.2 mL of a stock 50 mM solution of $KAuBr_4$ (in water only) was diluted to give 10 mL of a 1 mM solution, which was then added dropwise with stirring (to minimize large localized concentrations) to the 10 mL of amino acid solution at (20 ± 2) °C. The samples prepared in 0.05 M KOH therefore contained 0.5 mM of both amino acid and $KAuBr_4$.

2.2.2. Method B. 10 mL of a 1 mM amino acid solution in aqueous 0.05 M KOH solution was added dropwise to 10 mL of a 1 mM $KAuBr_4$ solution in 0.05 M KOH with stirring. Amino acid and gold reactants were therefore at a final concentration of 0.5mM in 0.05 M KOH.

2.3. Characterization. ***2.3.1. Transmission Electron Microscopy.*** Samples for TEM analysis were prepared by placing a drop of the gold suspension on a clean, dry 200 mesh copper grid coated with a carbon film. The sample deposited on the grid was allowed to dry in air for a few minutes, and excess solution was then removed using filter paper.

The size, morphology, and microstructure of the gold nanoparticle samples prepared as described above were studied using a JEOL 1010 transmission electron microscope equipped with a Gatan CCD camera (MSC SI0031) using Gatan Digital Micrograph software. The TEM was operated at an accelerating voltage of 100 kV.

2.3.2. Electrochemical Analysis. Voltammetric experiments were performed with a BAS Epsilon Electrochemical workstation that contained the RDE-2 accessory needed for rotating disk electrode (RDE) experiments. The electrochemical cell allowed reproducible positioning of the working, reference, and auxiliary electrodes and a nitrogen inlet tube. A 3 mm diameter glassy carbon (GC) electrode (BAS) was used as the working electrode for both the stationary and RDE electrode experiments. This electrode was polished with an aqueous 0.3 μm alumina slurry on a polishing cloth (Microcloth, Buehler), sonicated in deionized water for 5 min, and dried with tissue paper (Kimwipe) prior to use. The reference electrode was Ag/AgCl (aqueous 3 M KCl), and the auxiliary electrode was a coiled platinum wire. Initial voltammetric experiments were commenced after degassing the 0.05 M KOH electrolyte solutions with nitrogen for at least 10 min, and the solution was degassed continuously between voltammetric measurements to avoid large local concentrations and to provide homogeneity. Removal of oxygen was undertaken to avoid the presence of the oxygen reduction process in voltammograms and not to eliminate any oxygen participation in the gold nanoparticle formation process.

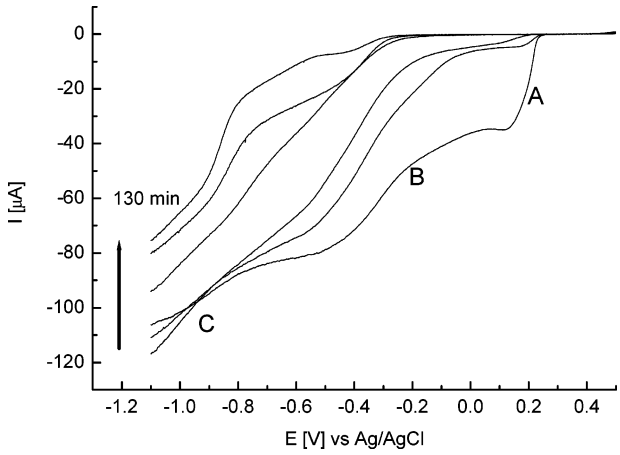

Figure 1. RDE voltammograms obtained at a GC electrode (scan rate = 50 mV s^{-1}, rotation rate = 2000 rpm) for the reduction of 0.5 mM $KAuBr_4$ in 0.05 M KOH after reaction times of 1, 5, 10, 25, 70, and 130 min. Arrow indicates increasing time.

2.3.3. UV−visible Spectrophotometry. Electronic spectra were obtained in a cell with a 1 cm path length with a Varian Cary 5 UV−visible spectrophotometer (Varian OS2 software). Spectra obtained with and without degassing of solutions with nitrogen were identical within experimental error.

3. Results and Discussion

3.1. Electrochemical Monitoring of Gold Particle Production. *3.1.1. Role of $KAuBr_4$.* 3.1.1.1. *In the Absence of Glycyl-L-tyrosine*. A highly basic solution is used for the gold nanoparticle formation process.[7] In 0.05 M KOH solution, dissolution of $KAuBr_4$ and simple dissociation into K^+ and $AuBr_4^-$ is unlikely, because above pH 10, formation of sparingly soluble solid $Au(OH)_{3(s)}$ is postulated to occur.[19] The time dependence of RDE voltammograms when $AuBr_4^-$ is added to 0.05 M KOH is complex (Figure 1). Several irreversible processes are detected. Each are attributed to reduction of different gold complexes to gold via a $Au^{III} + 3e^- \rightarrow Au^0$ process, with the total limiting current representing the concentration of dissolved Au(III). Initially, a sharp process A is detected at ~0.23 V, which is rapidly replaced by a more drawn-out process B at ~ −0.08 V. Finally, a process C at very negative potentials (−0.80 V) becomes dominant, which then slowly decreases with time, presumably as a solid form of gold ($Au(OH)_{3(s)}$ or $Au_{(s)}$—see later) is precipitated. These results imply that the formation of $Au(OH)_{3(s)}$ is slow and involves

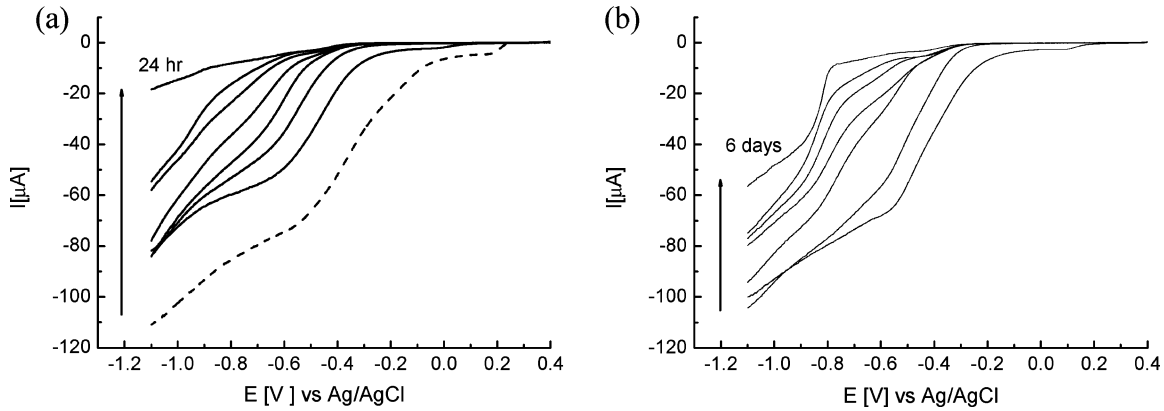

Figure 2. RDE voltammograms obtained at a GC electrode (scan rate = 50 mV s^{-1}, rotation rate = 2000 rpm) from a solution containing 0.5 mM $KAuBr_4$ and 0.5 mM glycyl-L-tyrosine in 0.05 M KOH: (a) Method A (see Materials and Methods section for experimental description) with reactant addition times of 3, 6, 10, 16, 30, and 50 min and 24 h. The dashed line is an RDE voltammogram obtained for 0.5 mM $KAuBr_4$ in 0.05 M KOH after 10 min. (b) Method B (see experimental description) with reactant addition times of 4, 17, 50, 80, 140, and 260 min, and 6 days.

gradual replacement of bromide by hydroxide, with the mixed hydroxide/bromide complexes formed as intermediates being more difficult to reduce than the $AuBr_4^-$ complex. A simple reaction scheme to explain the time dependence of the voltammetry is summarized in eqs 1−6

$$[AuBr_4]^- + OH^- \rightarrow [AuBr_3(OH)]^- + Br^- \quad (1)$$

$$[AuBr_3(OH)]^- + OH^- \rightarrow [AuBr_2(OH)_2]^- + Br^- \quad (2)$$

$$[AuBr_2(OH)_2]^- + OH^- \rightarrow [AuBr(OH)_3]^- + Br^- \quad (3)$$

$$[AuBr(OH)_3]^- + OH^- \rightarrow [Au(OH)_4]^- + Br^- \quad (4)$$

$$[Au(OH)_4]^- \rightarrow Au(OH)_{3(s)} + OH^- \quad (5)$$

$$2[AuBr_3(OH)]^- \rightarrow 2Au_{(s)} + 3Br_2 + 2OH^- \quad (6)$$

However, in 0.05 M KOH, bromine can participate in further redox chemistry to generate hypobromite and then bromate (see reverse of eqs 7 and 8),[20] and even bromide itself can react to generate bromate (see reverse of eq 9).[20] Thus the solution-phase redox chemistry is inherently complex, as indicated by the voltammetry (Figure 1).

$$2BrO^- + 2H_2O + 2e^- = Br_2 + 4OH^- \qquad E° = 0.450 \text{ V (SHE)} \quad (7)$$

$$BrO_3^- + 2H_2O + 4e^- = BrO^- + 4OH^- \qquad E° = 0.540 \text{ V (SHE)} \quad (8)$$

$$BrO_3^- + 3H_2O + 6e^- = Br^- + 6OH^- \qquad E° = 0.610 \text{ V (SHE)} \quad (9)$$

3.1.1.2. In the Presence of Glycyl-L-tyrosine. The formation of gold nanoparticles obviously requires reduction from an Au(III) precursor solution. RDE data (Figure 1) indicate that species formed at long times are much harder to reduce than species initially present. Consequently, nanoparticle formation via a reduction mechanism in the presence of glycyl-L-tyrosine is likely to depend on the identity of species present when glycyl-L-tyrosine is added to the Au(III) precursor solution and, hence, the order in which reagents are added. Thus, it is not surprising that addition of glycyl-L-tyrosine to a 0.05 M KOH solution to which $AuBr_4^-$ has already been added provided a very different rate of gold nanoparticle formation (Figure 2b) than the preferred order of reagent addition in which $KAuBr_4$ is added to a 0.05 M KOH solution containing glycyl-L-tyrosine (Figure 2a). For the case of addition of $KAuBr_4$ to a basic glycyl-L-tyrosine solution (denoted as Method A, see Materials and Methods), the extent of base hydrolysis is minimal and the most easily reduced bromide complexes are present at the maximum concentration. This results in a more rapid decrease in the voltammetric total limiting current response for the $Au^{III} \rightarrow Au^0$ process (see dashed line in Figure 2a with no glycyl-L-tyrosine present) as Au(III), most likely in the form of a more easily reduced bromide complex, is removed from solution to produce a product that cannot be electrochemically reduced. Indeed, the process detected in the absence of glycyl-L-tyrosine at 0.23 V, represented by the dashed line in Figure 2a, would seem to have vanished before an initial voltammogram can be obtained (∼3 min). The electrochemical reduction of the species left in solution also exhibits a dramatic negative shift in reduction potential. This shift in reduction potential is far more significant than that observed for $AuBr_4^-$ in base only (Figure 1) and suggests that the gold species in solution in this experiment is not a simple gold hydroxide/bromide complex but involves glycyl-L-tyrosine. This is expected, given that the highly basic 0.05 M KOH media used in the sample preparation ensures that the amine groups of the amino acid are significantly deprotonated, thereby enhancing the probability of complexation with Au(III). After the initial rapid decay, the solution composition then changes constantly with time, as evidenced by a continued negative shift in the reduction potential for the $Au^{III} \rightarrow Au^0$ process until nearly all Au(III) is removed from solution after 24 h.

If glycyl-L-tyrosine is added to a $KAuBr_4$ basic solution (denoted as Method B, see Materials and Methods), the initial significant decrease in the $Au^{III} \rightarrow Au^0$ voltammetric response as observed for Method A does not occur and the total $Au^{III} \rightarrow Au^0$ voltammetric response decreases at a much slower rate. Indeed, extensive removal of Au(III) from solution is only detected after 6 days of reaction time (Figure 2b).

3.1.2. Role of Glycyl-L-Tyrosine. Glycyl-L-tyrosine is oxidized irreversibly at a GC electrode (Figure 3). In the absence of Au(III), a well-defined peak is detected at 0.51 V under conditions of cyclic voltammetry. The peak height is a linear function of concentration over the range 0.1−1 mM. This process is assumed to be analogous to the irreversible electrochemical

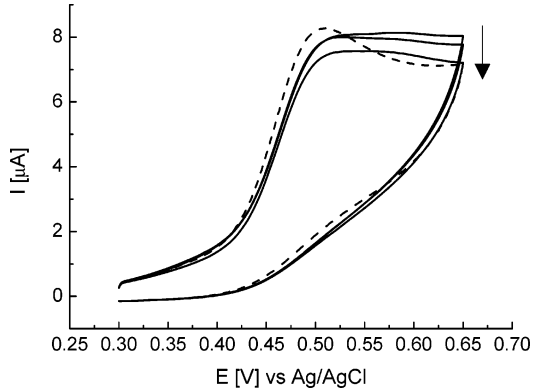

Figure 3. Cyclic voltammograms using a GC electrode with a scan rate of 50 mV s^{-1} in a solution consisting of 0.5 mM $KAuBr_4$ and 0.5 mM glycyl-L-tyrosine in 0.05 M KOH (solid lines) prepared by Method A (see experimental description) at reaction times of 5 and 30 min and 24 h. The dashed line is obtained in the presence of 0.5 mM glycyl-L-tyrosine in 0.05 M KOH. Arrow indicates increasing time.

oxidation of tyrosine.[21−24] In the presence of Au(III), only a small decrease in current magnitude is detected in the potential range where glycyl-L-tyrosine oxidation occurs. However, a change in wave shape is detected. RDE studies were also carried out to monitor the glycyl-L-tyrosine oxidation process, but such a subtlety in the oxidation response was not evident. Thus, while the maximum current for the glycyl-L-tyrosine oxidation response differed by only ca. 10% over the initial 24 h reaction period, the $Au^{III} \rightarrow Au^0$ voltammetric response is nearly absent over the same time period. It is also interesting to note that, at very early reaction times, there is an immediate 27% decrease in the total $Au^{III} \rightarrow Au^0$ response, which is accompanied by an immediate change in wave shape for the glycyl-L-tyrosine oxidation response. This suggests that the initial reaction between $AuBr_4^-$ or a minimally substituted hydroxide species with glycyl-L-tyrosine produces a species that cannot be electrochemically reduced in the potential range under study but does show an oxidation response different to that of free glycyl-L-tyrosine in solution. This newly generated species at early reaction times remains unchanged during the course of an experiment, as evidenced by the almost constant current magnitude observed over a 24 h period (Figure 3). Upon addition of a known concentration of glycyl-L-tyrosine to the reaction mixture after 24 h, the oxidation response increased in magnitude and, importantly, has the shape expected for free glycyl-L-tyrosine in solution.

It is also noteworthy, in the case of Method B, that the shape of the cyclic voltammetric glycyl-L-tyrosine response is completely unaffected by the presence of Au(III), but the peak height decreases by 20% over 24 h.

The voltammetric data imply that two major competing processes are associated with formation of elemental gold. Method A allows the most easily reduced $AuBr_4^-$ present at early reaction times (or a minimally substituted species such as $[AuBr_3(OH)]^-$) to be a major reactant. The latter species reacts immediately with glycyl-L-tyrosine to give a product which is undetectable by voltammetric methods and may be a form of glycyl-L-tyrosine−Au(III) complex that is extremely difficult to reduce. However, a derivative of glycyl-L-tyrosine can still be electrochemically oxidized, and this suggests that it is only changed in a subtle way upon the initial fast reaction with minimally hydrolyzed Au(III) species. In contrast, Method B requires that reduction should occur with more extensively hydrolyzed species (no free $AuBr_4^-$ is assumed to exist) and difficult-to-reduce species such as $[Au(OH)_4]^-$. This hinders

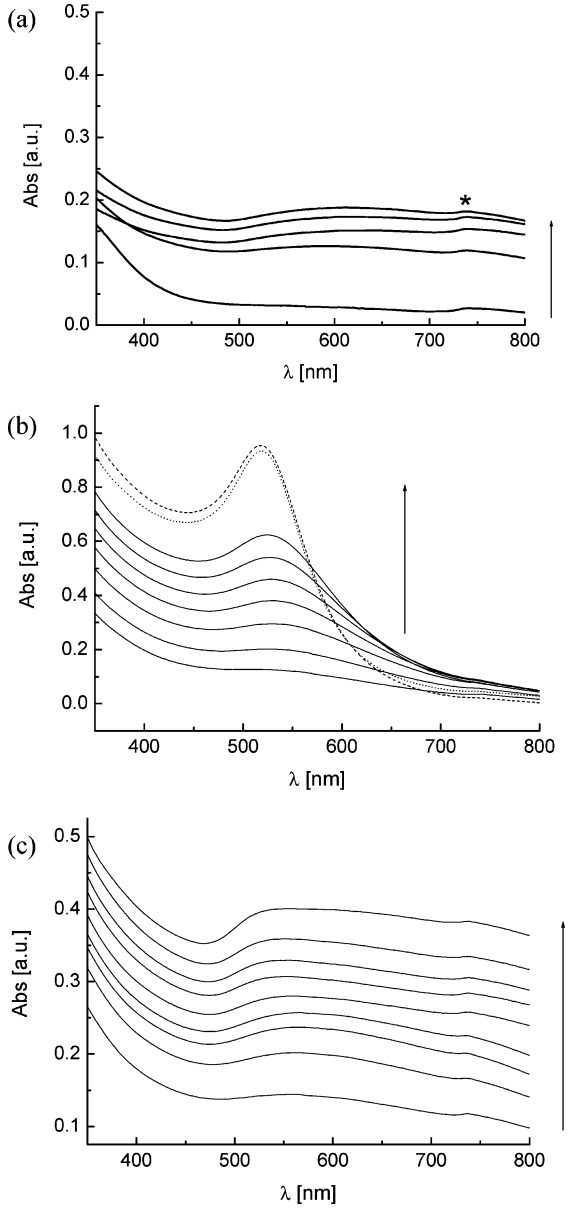

Figure 4. UV−visible spectra obtained for (a) 0.5 mM $KAuBr_4$ in 0.05 M KOH recorded after 3, 30, 55, 240, and 340 min of reaction; (b) Method A (see experimental description) with reactant addition times of 1, 3, 6, 10, 16, 30, and 60 min, and 24 h and 8 days; and (c) Method B (see experimental description) with reactant addition times of 4, 10, 20, 25, 55, 70, 100, 160, and 280 min. Arrows indicate increasing time.

both the initial fast reaction present in Method A, which is assumed to be rapid binding of glycyl-L-tyrosine to Au(III), and the rate of gold nanoparticle formation, as evidenced by the much slower decrease of the total $Au^{III} \rightarrow Au^0$ limiting current RDE voltammetric response with time (Figure 2b).

3.2. UV−visible Spectroscopy Analysis. Electrochemical methods can provide information on soluble reactant or product species during the course of an experiment but not on solid products formed, such as gold nanoparticles. Consequently, UV−visible spectra were employed to monitor gold nanoparticle formation in the constantly changing solution environment already probed by electrochemical experiments.

3.2.1. In the Absence of Glycyl-L-tyrosine. Electrochemical data showed that several Au(III) species are produced when $KAuBr_4$ is added to 0.05 M KOH (Figure 1). Time-resolved electronic spectra recorded (Figure 4a) reveal that the total absorbance in the visible region increases with time up to 6 h

and exhibits an increasing level of fine structure, which may be due to complex hydrolyzed Au(III) species or agglomerated gold nanoparticles. This response then decreased gradually with time, and a black precipitate was visually detected after 6 h. It was concluded from Energy Dispersive X-ray Analysis (EDAX) data of the black precipitate that elemental gold is formed from $KAuBr_4$ in 0.05 M KOH only, which suggests that the decrease in the total absorbance in the electronic spectra after 6 h is, at least in part, due to highly agglomerated gold precipitating out of solution. The feature detected at ~740 nm and marked with an asterisk (*) was present in all electronic spectra of other solutions examined. The same spectral feature was recorded with Varian Cary and Perkin-Elmer UV−visible spectrophotometers, and it is also not coincident with the instrument lamp-switching wavelength. A spectral feature of this type ~740 nm also has been observed in other studies where gold nanoparticles are produced using bioactive molecules,[25] which is not consistent with the classical Mie theory of spherical gold particles. It may be a manifestation of a specific form of aggregation;[26] however, the exploration of this requires more sophisticated modeling techniques than Mie theory and is, thus, beyond the scope of this study.

3.2.2. In the Presence of Glycyl-L-tyrosine. Electrochemical data revealed that speciation plays a critical role in the rate of consumption of dissolved Au(III) species. With Method A, time-resolved UV−visible spectra exhibit a gold plasmon resonance peak at 530 nm after only 6 min of reaction time (Figure 4b). The hypothesis that colloidal gold is rapidly formed under these conditions correlates with the time-resolved RDE experiments, which indicated the initial formation of a product that could not be electrochemically reduced. This plasmon resonance absorbance slowly increases in intensity over the next 24 h, indicating that progressively more extensive nanoparticle formation occurs (also supported by the time-resolved TEM images discussed below). The maximum wavelength position also shifts from 530 to 518 nm over this time period, which coincides with the gradual consumption of Au(III) species, as detected voltammetrically. From 24 h to 8 days, the plasmon resonance intensity remains essentially constant. This is expected on the basis of the voltammetric data, which indicated that almost complete consumption of Au(III) species had occurred after 24 h. Electrochemical data imply that the solution environment in which the nanoparticles are forming is continuously changing in both concentration and composition. This change also coincides with a narrowing and blue shifting of the plasmon resonance peak and a reduction in the intensity of the spectral feature observed ~740 nm.

In the case of Method B, only minimal evidence for a gold nanoparticle surface plasmon peak is obtained (Figure 4c). In this case, the electronic spectra are dominated by an extended region of absorbance from 540 to 720 nm in the absence of glycyl-L-tyrosine, although the intensity of the absorbance is larger at all wavelengths. As the experiments of Zhong et al.[26] proved, broad absorption in the 540−720 nm region may result from a superposition of plasmon resonances arising from nanoparticle aggregates with a distribution of both particle size and interparticle separation distance (the superposition consists of distributions of transverse and longitudinal plasmon resonances). The absorption intensity at 520 nm is less than that observed with Method A. This suggests that fewer gold nanoparticles are formed with Method B, as deduced from the electrochemical data, which showed that a significant amount of Au(III) remained in solution even after 6 days of reaction. Therefore, it is concluded that the speciation of gold plays a role not only in the rate and extent of nanoparticle formation but also in the resultant dispersion of nanoparticles in solution.

Consistent with the importance of gold(III) speciation, as deduced from voltammetric data, it was noted that the extent of gold nanoparticle formation formed with Method B can be increased significantly by addition of KBr (5 mM) to the $KAuBr_4$ (in 0.05 M KOH) solution prior to addition of glycyl-L-tyrosine. Examination of electronic spectra in Figure S1 (see Supporting Information) reveals that a distinct gold plasmon resonance peak is detected after only 40 min of reaction time in the presence of excess bromide. Concomitantly, the extended absorbance region from 540 to 800 nm is absent. This result further emphasizes that the speciation of the gold complex is critical with respect to not only the rate and extent of reduction to elemental gold and nanoparticle formation but also their dispersion in solution.

In the case of Method A, addition of excess bromide (5 mM) resulted in extensive precipitation that was visible by eye after 110 minutes. Time-resolved UV−visible spectra (Figure S2) exhibited a broad absorbance over the range of 500−800 nm, indicative of the presence of agglomerated gold. A slow decrease of absorbance was found with time, as highly agglomerated gold fell out of the solution. Thus, the presence of excess bromide in Method A may accelerate the rate of gold nanoparticle formation to the point where agglomeration becomes a significant problem.

3.3. TEM Analysis. In situ voltammetric and electronic spectral data have shown that gold nanoparticle formation from the aqueous peptide system represents a complex and dynamic system. However, these techniques do not allow the physical nature of gold nanoparticles formed to be deduced. Time-resolved TEM analysis was therefore employed to probe the structures of the colloidal or nanoparticle species formed in solutions prepared with glycyl-L-tyrosine. The assumption is made in interpreting these images that removal of solvent and reagents does not significantly perturb the nature of the solid. Times chosen for TEM analysis were governed by matching those values where specific features were detected in time-resolved UV−visible and voltammetric measurements.

Parts a−c of Figure 5 provide representative TEM images of a sample prepared by Method A, which was deposited on the TEM grid at a reaction time of 40 min, while Figure 5d presents an image obtained after a reaction time of 7 days. Immediately apparent in Figure 5a is the presence of an extended gellike species, which contains nanoparticle clusters. The images in parts b and c of Figure 5 also indicate the coexistence of highly amorphous regions that appear to have high electron density and regions containing clusters of gold nanoparticles, with isolated nanoparticles present in the matrix present between these regions. The higher resolution image in Figure 5c reveals that the particles are concentrated in a small volume element, and there is a suggestion of some level of separation, consistent with the formation of "nanonetworks" of a similar type to those reported by Gomez et al.[27] The existence of elemental gold in the solid formed at this time was previously deduced by noting the plasmon resonance peak present at early reaction times (<40 min). Figure 5d represents a micrograph image of solid after a reaction time of 7 days. With longer reaction times, the system transforms into a highly dispersed solution of gold nanoparticles, which exhibits monodispersity consistent with previously published data.[28]

TEM images of solid isolated from the Method B reaction are significantly different after a reaction time of 4 days (Figure

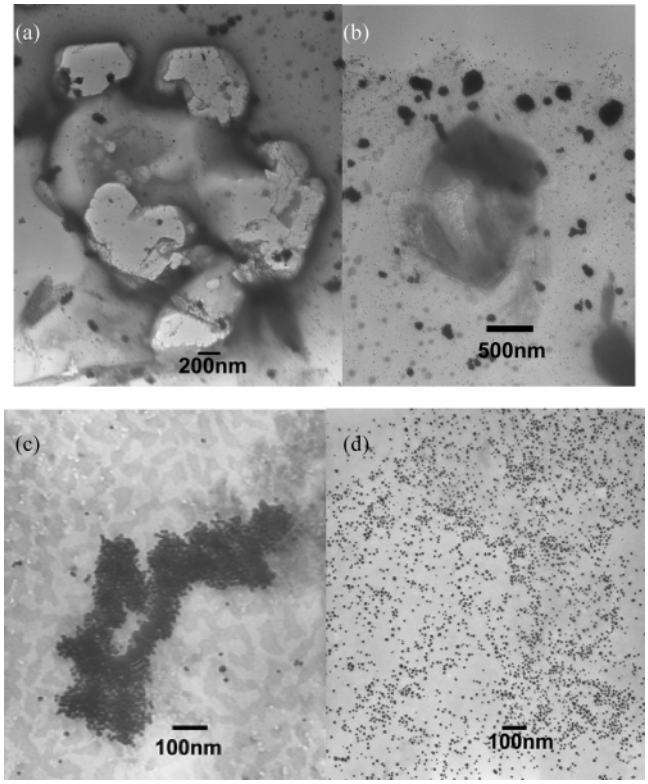

Figure 5. Representative TEM micrographs of a glycyl-L-tyrosine sample prepared via Method A (see experimental description) taken at reaction times of (a,b,c) 40 min and (d) 7 days.

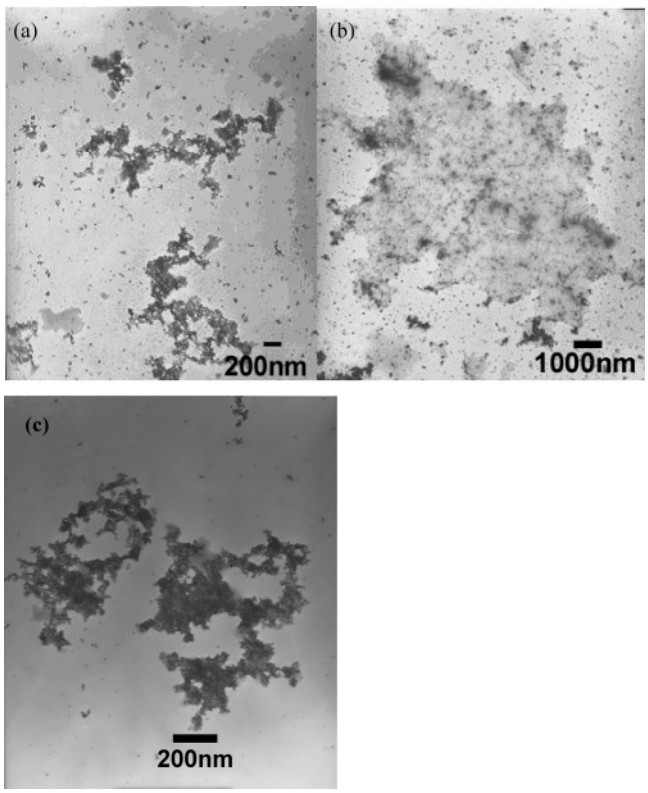

Figure 6. Representative TEM micrographs of a glycyl-L-tyrosine sample prepared via Method B (see experimental description) taken at a reaction time of 4 days.

6). It is immediately apparent that the nanoparticles formed are not completely dispersed and that there are numerous clusters present that do not show the separation between particles observed for early reaction times in Method A (Figure 5c). The agglomerated particles seen here are assumed to be related to those that give an extended region of absorbance from 540 to 800 nm in electronic spectra (Figure 4c).

4. Mechanism

What is clearly evident is that the formation of elemental gold does not involve a stoichiometric three-electron reaction between Au(III) and glycyl-L-tyrosine analogous to the one-electron reduction process postulated to occur in the case of Ag nanoparticle formation[29] (eq 10).

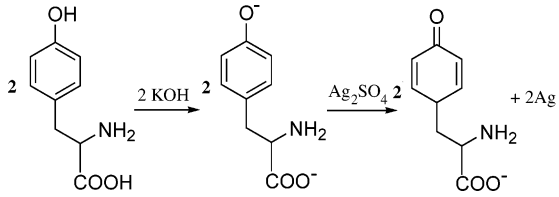

(10)

The amount of glycyl-L-tyrosine needed to cap the 10 nm gold nanoparticles formed is calculated to only consume a minimal amount of this peptide. The data obtained for the gold system infers that that this peptide may not be the dominant reductant, which implies that bromide is involved in the reduction of Au(III) to gold nanoparticles. In principle, complete consumption of Au(III) by bromide can be expected to occur by an overall reaction of the kind

$$2[AuBr_4]^- \rightarrow 2Au + 2Br_3^- + Br_2 \qquad (11)$$

where further redox reactions leading to hypobromite and bromate as outlined via the reverse of eqs 7−9 may occur and, hence, facilitate the reduction of $AuBr_4^-$ and mixed ligand complexes containing bromide by the following process

$$2[Au(OH)_3Br]^- = 2Au_{(s)} + Br^- + BrO_3^- + 3H_2O \qquad (12)$$

or other related reactions.

A comparison of the rate of reduction of the $Au^{III} \rightarrow Au^0$ response with Methods A and B also suggests that bromide reduces Au(III)−glycyl-L-tyrosine complexes more easily than a gold hydroxide complex such as $[Au(OH)_4]^-$. Addition of excess bromide to the reaction mixture (Method A) increased the rate of reaction to the point where it resulted in severe agglomeration of the nanoparticles, which precipitate out of solution.

The combination of data obtained from in situ electrochemical, electronic spectral, and ex situ imaging techniques suggests that the formation of gold nanoparticles in the glycyl-L-tyrosine system proceeds via the following processes:

(1) **The addition of the Au(III) precursor to a basic solution of glycyl-L-tyrosine results in the formation of an extended matrix of gold bromide/hydroxide/amino acid complexes of differing composition.** Given that Au(III) will form square planar complexes, it is reasonable to assume that, in this environment, the Au(III) may bind readily to the amino acid and will cross-link the amino acid molecules, thus forming large polymeric clusters as postulated in structure 2. The complete complexation of Au(III) with glycyl-L-tyrosine in this form is unlikely to occur, and the presence of several different soluble Au(III) species containing a mixture of the amino acid, bromide, and hydroxide is expected.

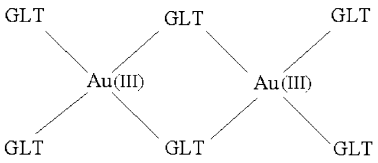

Structure 2: Cross linked amino-acid-glycyl-L-tyrosine (GLT)-Au(III) species.

Such a structural change, as well as the formation of other mixed complexes containing glycyl-L-tyrosine, may be responsible for the change in shape of the glycyl-L-tyrosine oxidation response, as well as the initial decrease and the considerable negative shift in the $Au^{III} \rightarrow Au^0$ response for the Au(III)−glycyl-L-tyrosine containing solution (Figure 2a). Cross-linking of this kind with aqueous metal cations that favor square planar geometry is well-known.[30] Because of the relatively low concentrations of the reactants and the low molecular weight of the amino acid, the system is not expected to form a true gel, but rather polymerization will result in the formation of globules suspended in solution, such as those reported by Chow and Zukoski.[11] Such globules can be clearly seen from the TEM images taken at early reaction times for Method A (Figure 5 parts a and b).

(2) **Au(III) ions are reduced within the matrix to form nuclei.** If the local concentration of Au(III) in the cluster is sufficiently high, and the reduction process reasonably facile, nucleation is expected to occur, forming nanocrystals of Au(0) within the cluster. The reduction process apparently does not involve a stoichiometric reaction between Au(III) and glycyl-L-tyrosine and most likely involves free bromide in solution. Images in parts a−c of Figure 5 imply that, once formed, these gold nuclei remain bound. The binding of amino acid molecules to gold nanoparticles is well-documented.[6,8] As Au(III) is reduced and coalesces into a crystal lattice, the frustrated coordination of the Au atoms on the perimeters of the nuclei will be receptive to donor bonds from the amino acid−Au(III) matrix, which will bind the nuclei into the cluster structure.

(3) **The nuclei formed rapidly accrete Au(III) species, forming nanoparticles which are bound into the matrix.** At longer times, the nuclei contained in the cluster will then accrete Au(0) by further reduction and deposition in an autocatalytic process[31] promoted by the particle surfaces. The linking of the particle surfaces to the amino acid−Au(III) cross-linked matrix provides a convenient pathway for depositional growth, as the matrix into which the particles are bound fixes Au(III) species in close proximity to the particle surfaces. This depositional growth will fill out the particle structure, forming spherical particles as the particles seek to balance the lattice stabilization energy with the particle surface tension by minimizing surface curvature, and thereby forming spherical shapes[32] as indicated by the UV−visible spectrophotometric data (Figure 4b). Facile binding and further reduction, will then result in the dense particle cluster illustrated in Figure 5c. The frustrated coordination of the surface Au atoms resulting from the relatively high surface curvature of nanoparticles of the dimensions observed (∼9 nm) is expected to lead to binding of the particles to the residual amino acid−Au(III) matrix. However, as the depositional growth process proceeds, the Au(III) binding the cluster together is consumed as it is accreted onto the particle surfaces. Assuming facile deposition, such that the vast majority of the Au(III) in the nanoparticle cluster is eventually converted to Au(0), the net result will be the consumption of the majority of the Au(III), which provides the gold metal cluster with its structural rigidity by cross-linking the amino acid molecules. For an amino acid such as glycyl-L-tyrosine, which contains several sources of mobile pi-electrons, including an aromatic ring, which can stabilize the oxidized form, the consumption of Au(III) within the nanoparticle cluster will be slow but becomes complete after ∼24 h (Figure 2c), as evidenced by the nearly complete absence of any $Au^{III} \rightarrow Au^0$ response at this time.

(4) **Continued reduction and subsequent accretion of Au(III) results in the collapse of the matrix into a dispersion of isolated gold nanoparticles.** The globules/clusters are present in a continually changing solution environment, as seen from the voltammetric data in Figure 2a. The continued formation of gold nanoparticles with time, as observed by electronic spectra, suggests that the species left in solution (complexes of mixed composition) play a critical role in nanoparticle formation. The species that are left in solution interact with these globules/clusters to form more nanoparticles, thereby consuming any Au(III) within the cluster. This destroys the cross-linking with the amino acid and, therefore, the structural rigidity of the cluster. This results in a well-dispersed gold nanoparticle solution, as seen from the narrow and intense plasmon resonance peak in Figure 4b, the eventual disappearance of the spectral feature from 720 to 800 nm (Figure 2c) assumed to arise from agglomerated gold, and the TEM images recorded in Figure 5d. It is interesting to note that well-dispersed nanoparticles are only observed after extensive consumption of Au(III) species in solution. However, the shape of the glycyl-L-tyrosine oxidation response observed in Figure 3 remains even after 8 days, when a solution of well-dispersed gold nanoparticles has formed. This implies that the residual Au(III) species that are still present in solution (see Figure 2a, the $Au^{III} \rightarrow Au^0$ response has not completely disappeared) are still complexed with the peptide in some manner that affects its electrochemical oxidation response compared to free glycyl-L-tyrosine in solution. This change of shape may be due to several different types of complexes containing Au(III), bromide, hydroxide, and glycyl-L-tyrosine and may even involve the electrochemical oxidation of the capping layer of glycyl-L-tyrosine on the gold nanoparticles themselves.

Conclusions

The novel combination of insights gained from analysis of electrochemical and UV−visible data and inspection of TEM images allows a particle formation mechanism to be formulated which differs considerably from traditional paradigms. The high pH conditions favor, upon addition of the bromoaurate solution, formation of gellike matrixes of varying compositions of the amino acid cross-linked by Au(III), with the cross-linking most likely occurring via the amine/amide groups. This composition is only favored if hydrolysis of $KAuBr_4$ is minimized, since any extensive gold hydroxide complex formation greatly retards this initial step. The cross-linking can fix the Au(III) species within close proximity, and in some regions of the matrixes, the requirements for nucleation are satisfied. Thus, nuclei will form which are still bound into the matrixes, and their surfaces will then catalyze depositional growth from reduction of other Au(III) species in solution, possibly facilitated by the presence of free bromide. Bromide is a likely participant in the reduction process, given that a three-electron stoichiometric reaction between Au(III) and glycyl-L-tyrosine is not likely. If the reduction step is relatively facile, this results in the vast majority of the Au(III) bound into the matrixes being consumed, thus removing the links which provide the matrixes with their structural (semi)rigidity, and consequently, collapse into a dispersion of gold nanoparticles will occur. This mechanism

also provides a pathway for capping of the particles, which stabilizes them with respect to aggregation, because during the depositional growth stage, the amino acid bound to depositing Au species may bind to the particle surface.

Supporting Information Available: Supporting information available for this document includes UV−visible spectra obtained after the addition of a basic solution of glycyl-L-tyrosine to a basic solution of $KAuBr_4$ at times 40 min and 4 days, as well as UV−visible spectra obtained after the addition of an aqueous solution of $KAuBr_4$ to a basic solution of glycyl-L-tyrosine at various times. This material is available free of charge via the Internet at http://pubs.acs.org.

References and Notes

(1) Daniel, M.-C.; Astruc, D. *Chem. Rev.* **2004**, *104* (1), 293
(2) Shankar, S. S.; Rai, A.; Ankamwar, B.; Singh, A.; Ahmad, A.; Sastry, M. *Nature Mater.* **2004**, *3*, 482.
(3) Chandran, S. P.; Choudhary, M.; Pasricha, R.; Ahmad, A.; Sastry, M. *Biotechnol. Prog.* **2006**, *22*, 577.
(4) Ahmad, A.; Senapati, S.; Khan, M. Islam; Kumar, R.; Sastry, M. *Langmuir* **2003**, *19*, 3550.
(5) Zhou, Y.; Chen, W.; Itoh, H.; Naka, K.; Ni, Q.; Yamane, H.; Chujo, Y. *Chem. Commun.* **2001**, 2518.
(6) Mandal, S.; Selvakannan, P. R.; Phadtare, S.; Pasricha, R.; Sastry, M. *Proc. Ind. Acad. Sci. (Chem. Sci.)* **2002**, *114* (5), 513.
(7) Shao, Y.; Jin, Y.; Dong, S. *Chem. Commun.* **2004**, 1104.
(8) Selvakannan, P. R.; Mandal, S.; Phadtare, S.; Gole, A.; Pasricha, R.; Adyanthaya, S. D.; Sastry, M. *J. Colloid Interface Sci.* **2004**, *269*, 97.
(9) Shankar, S. S.; Rai, A.; Ahmad, A.; Sastry, M. *Chem. Mater.* **2005**, *17*, 566.
(10) Turkevich, J.; Stevenson, P. C.; Hillier, J. *J. Phys. Chem.* **1953**, *57*, 670.
(11) Chow, M.; Zukoski, C. *J. Colloid Interface Sci.* **1994**, *165*, 97.
(12) Zhang, P.; Kim, P. S.; Sham, T. K. *Appl. Phys. Lett.* **2003**, *82*, 1470.
(13) Ma, H.; Yin, B.; Wang, S.; Jiao, Y.; Pan, W.; Huang, S.; Chen, S.; Meng, F. *ChemPhysChem* **2004**, *5*, 68.
(14) Ingram, R. S.; Hostetler, M. J.; Murray, R. W.; Schaaf, T. G.; Khoury, J. T.; Whetten, R. L.; Bigioni, T. P.; Guthrie, D. K.; First, P. N. *J. Am. Chem. Soc.* **1997**, *119*, 9279.
(15) Chen, S.; Murray, R. W.; Feldberg, S. W. *J. Phys. Chem. B* **1998**, *102*, 9898.
(16) Miles, D. T.; Leopold, M. C.; Hicks, J. F.; Murray, R. W. *J. Electroanal. Chem.* **2003**, *554*, 87.
(17) Quinn, B. M.; Liljeroth, P.; Ruiz, V.; Laaksonen, T.; Konturri, K. *J. Am. Chem. Soc.* **2003**, *125*, 6644.
(18) Jimenez, V. L.; Georganopoulou, D. G.; White, R. J.; Harper, A. S.; Mills, A. J.; Lee, D.; Murray, R. W. *Langmuir* **2004**, *20*, 6864.
(19) Kelsall, G. H.; Welham, N. J.; Diaz, M. A. *J. Electroanal. Chem.* **1993**, *361*, 13.
(20) Dobos, D. In *A Handbook for Electrochemists in Industry and Universities*; Elsevier: Amsterdam−New York, 1975.
(21) Ogura, K.; Kobayashi, M.; Nakayama, M.; Miho, Y. *J. Electroanal. Chem.* **1999**, *463*, 218.
(22) Marx, K. A.; Zhou, T. *J. Electroanal. Chem.* **2002**, *521*, 53.
(23) Jin, G.-P.; Lin, X.-Q. *Electrochem. Commun.* **2004**, *6*, 742.
(24) Xu, Q.; Wang, S.-F. *Microchim. Acta* **2005**, *151*, 47.
(25) Pal, A. *J. Nanoparticle Res.* **2004**, *6*, 27.
(26) Zhong, Z.; Patskovsky, S.; Bouvrette, P.; Luong, J.; Gedanken, A. *J. Phys. Chem. B* **2004**, *108*, 4046.
(27) Gomez, S.; Pilippot, K.; Colliere, V.; Chaudret, B.; Senocq, F.; Lecante, P. *Chem. Commun.* **2000**, 1945.
(28) Bhargava, S. K.; Booth, J. M.; Agrawal, S.; Coloe, P.; Kar, G. *Langmuir* **2005**, *21*, 5949
(29) Selvakannan, P.; Swami, A.; Srisathiyanarayanan, D.; Shirude, P.; Pasricha, R.; Mandale, A.; Sastry, M. *Langmuir* **2004**, *20*, 7825.
(30) Oyrton, A. C. M.; Airoldi, C. *J. Colloid Interface Sci.* **1999**, *212*, 212.
(31) Turkevich, J. *Gold Bull.* **1985**, *18* (3), 86.
(32) Moody, M.; Attard, P. *J. Chem. Phys.* **2002**, *117* (14), 6705.